Lawrence Berkeley National Laboratory

Title
Assessing the geomechanical stability of interbedded hydrate-bearing sediments under gas production by depressurization at NGHP-02 Site 16

Permalink
https://escholarship.org/uc/item/28s3c88r

Authors
Lin, Jeen-Shang
Uchida, Shun
Myshakin, Evgeniy M
et al.

Peer reviewed

Assessing the geomechanical stability of interbedded hydrate-bearing sediments under gas production by depressurization at NGHP-02 Site 16

Jeen-Shang Lin, Shun Uchida, Evgeniy M. Myshakin, Yongkoo Seol, Jonny Rutqvist, Ray Boswell

Abstract

Establishing the geomechanical stability of marine sediments in the vicinity of a production well is one of the key design considerations in planning offshore gas production from marine hydrate reservoirs. This paper presents an assessment of the sediment stability at India's National Gas Hydrate Program, Expedition 2 (NGHP-02) Site 16 Area B offshore eastern India, for which gas production is to be carried out by depressurization. One important feature of the study is that extensive calibration of constitutive model parameters has been conducted based on laboratory test data from pressured core samples. From analysis perspective, the site is challenging because the hydrate reservoir consists of thin layers of hydrate-bearing sands interbedded with mud. Moreover, depressurization at the depth of a reservoir more than 2750 m below sea surface will lead to a pore pressure drop, and accordingly an effective confining stress increase as high as 25 MPa. In dealing with thin interbedded hydrate-bearing strata, meshing requirements for flow and geomechanical analysis are quite different from those for reservoirs with thicker massive layers, An axisymmetric model and one-way coupling simulations were thus adopted for this study, in which the geomechanical study utilizes pore pressure and hydrate saturation output from the flow study, but the flow study does not takes the porosity changes from the geomechanical analysis. Instead, the reduction of porosity due to sediment deformation in the flow study is based on a pressure-dependent pore compressibility relationship derived from geomechanical modeling. The rationality is validated through back computing the pore compressibility from the geomechanical deformation results. The study shows that large compression in the reservoir will result in movement of the sediments from above and below, as well as laterally in smaller magnitudes; and the sediment is deemed stable during the gas production period.

Keywords: Gas hydrates, Geomechanical analysis, Constitutive model, Marine gas hydrate deposits, India National gas hydrate program

1. Overview

One of the key design considerations in planning offshore gas production from marine hydrate reservoirs is how the geomechanical response of the sediments might affect well instability and casing deformation (Moridis et al., 2011). This paper presents a geomechanical study for NGHP-02 Site 16 (Collett et al., this volume; Kumar et al., this volume; Shukla et al., this volume) offshore eastern India during the early stage of gas production by depressurization. Two companion papers discuss

the modeling of gas production (Myshakin et al., this volume) and modeling of sand migration and its impacts (Uchida et al., this volume). Geomechanical test results with NGHP pressure cores are separately presented by Yoneda et al. (this volume a). Because the hydrate reservoir unit is located between 2819.3 m and 2843.4 m below the sea level, hydrate dissociation induced by depressurization requires a pressure drop of up to 25 MPa. This is a substantial pressure reduction; for instance, the pressure reduction for the Eastern Nankai Trough gas production test was less than 10 MPa (Yamamoto et al., 2014). Site 16 is also challenging from a modeling perspective because the hydrate reservoir under consideration consists of numerous thin layers of hydrate bearing strata interbedded with find grained layers (Boswell et al., this volume). Recent advances in laboratory testing (Choi et al., 2014; Hyodo et al., 2014; Masui et al., 2005; Miyazaki et al., 2011; Waite et al., 2009; Yoneda et al., 2017), critical state constitutive modeling (Uchida et al., 2012; Lin et al., 2015), and coupled geomechanical modeling (Kim et al., 2012; Rutqvist, 2017; Rutqvist et al., 2012) help the present study to overcome the challenging complexities
in geomechanics simulation of thinly interbedded hydrate-bearing reservoirs under depressurization.

A fully coupled study that ties together the flow and geomechanical analysis is the preferred modeling framework (Klar et al., 2013; Rutqvist et al., 2009). However, for this study, because of the thin interbeds, the meshing requirements for flow and geomechanical analyses are very different. Specifically, in order to accurately capture flow characteristicsduring the dissociation process, the reservoir unit has to be divided into thin layers of 0.1 m. For the geomechanical study, a much coarser mesh must be used in order to obtain viable simulation run times. A critical issue in the mechanical modeling is to ensure that the boundary between mud and sands are properly incorporated. With different mesh geometries, a coupled flow and geomechanical study would not be efficient. Thus, a two-way coupling between the flow and the geomechanical analysis was not adopted. Instead, this study adopts a one-way coupling approach in which the geomechanical study utilizes pore pressure and hydrate saturation output from the flow study, but the flow study does not takes directly the porosity changes from the geomechanical analysis. This reduction of porosity due to sediment deformation in the flow study is based on a pressure-dependent pore compressibility relationship derived from geomechanical modeling. Then at the end of the study, it is further validated with results from geomechanical modeling.

This paper is organized as follows: first, the modeling framework overview is presented, which is followed by discussion of the modeling parameter determination based on the available experimental data. Then the computational model including the boundary conditions is described before results of the modeling in terms of subsidence, lateral movement, shear

stresses are summarized with stability assessment. Validation of the one-way coupled approach is addressed at the end.

2. Modeling framework

Based on the logging data, the sediment at the site is divided into 5 units as detailed in Table 1. The hydrate rich reservoir lies within Unit 4. This unit consists of thin layers of hydrate rich sands that are interbedded with muds. Fig. 1 shows that the hydrate rich sands were simplified and represented by 18 layers in the study, and the hydrate saturation of 80% is assigned to each of them initially using the methods as described in Boswell et al. (this volume).

Table 1. NGHP-02 Site 16 site B geological units.

Major Model Unit	Sub-seafloor Depth[a] (m)	Thickness (m)	Porosity, φ_0	Saturated density (kg/m^3)
UNIT 1: uniform marine mud with no hydrate	0.0–151.0	151.0	0.67	1563.9
UNIT 2: uniform marine mud with fracture filled gas hydrate	151.0–244.0	93.0	0.66	1580.1
UNIT 3: uniform marine mud with no hydrate	244.0–272.8	28.8	0.71	1499.1
UNIT 4: Interbedded hydrate-bearing sand and hydrate-free mud	272.8–296.9	24.1	0.4	2001.6
UNIT 5: uniform marine mud with no hydrate	Below 296.9		0.53	1790.9

[a]

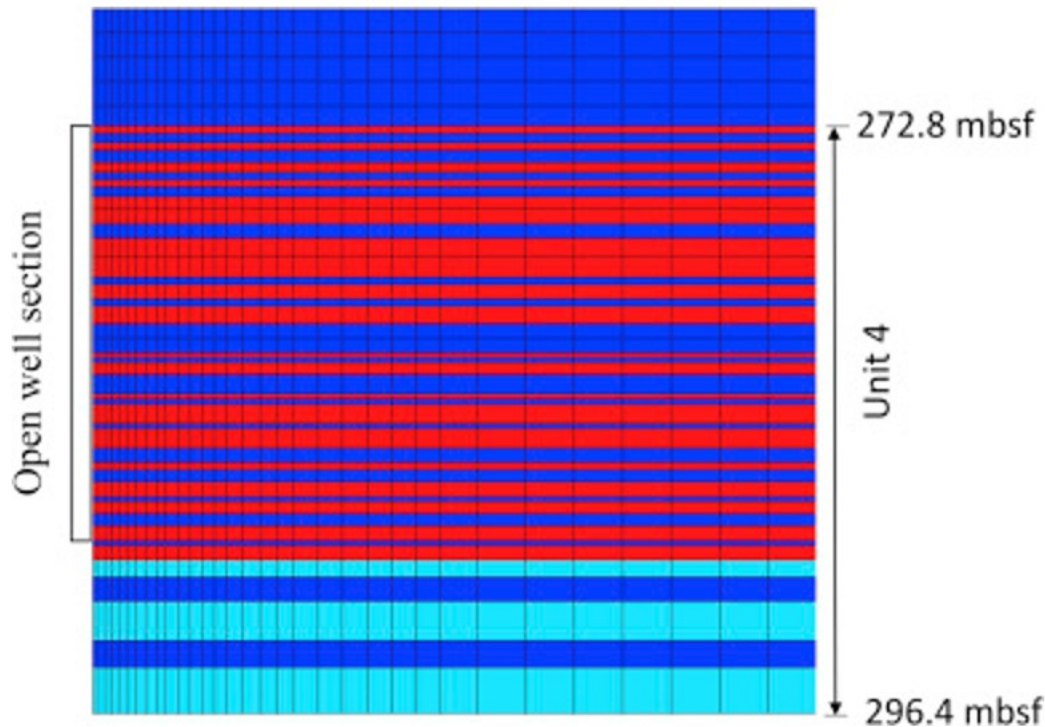Sea floor is located 2546.5 m below sea surface.

Fig. 1. Location of the completed well (open section) and the simplified 18 thin strata of hydrate-bearing sands (red) interbedded with muds (blue), underlain by 3 water-bearing sand strata (indigo) in Unit 4. The open section of the well runs from the top of first to the bottom of the seventeenth hydrate-bearing sand strata.

For the study, the production test well is modeled as a vertical well with both the hydrate-bearing sands and the mud-rich interbeds are open to the wellbore between the depths 272.8 and 289.8 mbsf. This design leaves the basal hydrate-bearing sand and all subjacent water-bearing units with no direct connection to the wellbore. The thin mud layer and 18th hydrate layer, having the initial effective intrinsic permeability of 1 md, protect the well waterinflows from below. The last 18th hydrate layer remains intact and there is no highly permeable hydraulic communication between the underlying aquifer and the well. This is further discussed in Myshakin et al. (this volume). The flow simulation induces depressurization by imposing a constant pressure of 3.0 MPa just above the top of Unit 4 in the open section of the well, and assign the open section of the well a high vertical permeability representing the wellbore itself.

For this study, TOUGH + Hydrate, or T + H (Moridis et al., 2008), was used for the flow study, while the geomechanical study was carried out in FLAC3D (Itasca Consulting Group, 2012) with the user implemented constitutive model. The basic modeling framework of linking T + H to FLAC3D can be found in (Rutqvist and Moridis, 2009), which has been applied for a number of studies on geomechanical aspect of gas hydrates (Kim et al., 2012; Rutqvist et al., 2009). The geomechanical analysis presented in this paper is carried out via one-way coupling between multiphase flow analysis

of T + H and geomechanical analysis using FLAC3D. The essence of two-way coupling is, at each time step, to adjust the porosityof the sediment for the next step in the flow study according to the deformation obtained in the geomechanical study. To carry out a credible one-way coupling, the porosity change in the flow study is introduced but in a different manner as stated below. At specified times, the pore pressure, p, and the hydrate saturation, S_H, obtained from the flow simulation are output for use by the geomechanical study, but the geomechanical simulation results are not used by the flow simulation. Instead, the flow study uses a pressure-dependent pore compressibility from laboratory consolidation tests to model the effect of reservoir volumetric deformation on fluid mass balance that is incurring during depressurization (Myshakin et al., this volume). The sediment volumetric deformation is derived from porosity change, which is a function of pore compressibility and pressure difference, as shown below

(1)$\varphi = \varphi_o \exp(\alpha \Delta p)$

where α is pore compressibility, φ_o and φ are, respectively, the porosities before and after a pore pressure change,Δp. At the completion of the study, the validity of the pressure-dependent pore compressibility used is evaluated against the resulting deformation from the geomechanical analysis to evaluate the validity of the one-way coupling approach. The flow simulation used $\alpha = 1.3 \times 10^{-8} (Pa^{-1})$ based on the consolidation test data (Yoneda et al., this volume a) as discussed in Boswell et al. (this volume) and Myshakin et al. (this volume).

3. Soil constitutive model

The core of a geomechanical analysis is the soil constitutive model. This study adopts a sub-loading critical state model for methane hydrate bearing soils (MHBS) (Uchida et al., 2012). There are essential stress-strain characteristics that a proper constitutive model must capture: elastic and plastic deformation of the sediment under both pressure and shear, dilatancy, strain-softening, and the strength under sustained shear strain often referred to as the critical state. Plastic deformation under pressure is also known as volumetric yielding. Under high depressurization, the sediments are subjected to large isotropic loading, which induces volumetric yielding and even grain crushing. Upon volumetric yielding, volumetric deformation accelerates under a given incremental stress since the deformation is no longer elastic. Therefore, it is essential to capture volumetric yielding for accurate prediction of sediment deformation. As illustrated in Fig. 2, without introducing a yield surface to define when volumetric yielding occurs, conventional Mohr-Coulomb failure criterion is not capable of capturing volumetric yielding, and the increase in the mean effective stress only makes the soil more stable. For this reason, the use of a constitutive model such as the critical state model that incoporates volumetric yielding is essential.
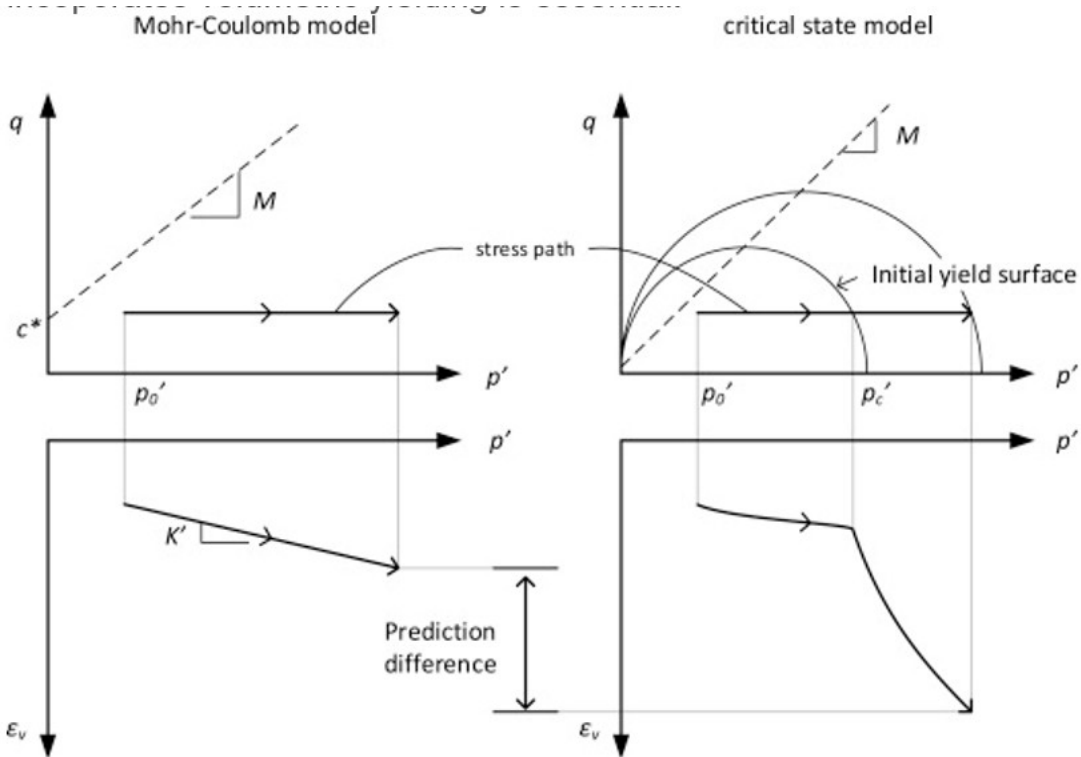
Fig. 2. The importance of incorporating volumetric yielding in constitutive model illustrated by the contrast of Mohr-Coulomb model versus Critical state model.

The present MHBS model is built on the modified Cam clay model (Roscoe and Burland, 1968), of which the critical state concept is an essential part. The Cam clay (Schofield and Wroth, 1968) components that are preserved include the following:

1)

The normal consolidation line that is defined by

$$(2) \quad v = N - \lambda \cdot \ln(p')$$

where p' is the effective confining pressure, v is the specific volume ($v = 1 + e$) with e being the void ratio, N is v at $p' = 1$ MPa, and λ is the slope. The unload-reload slope is κ.

2)

The critical state line is defined by q_{CS} and v_{CS} as follows,

$$(3) \quad q_{CS} = M \cdot p'$$

$$(4) \quad v_{CS} = \Gamma - \lambda \cdot \ln(p')$$

where q_{CS} and v_{CS} are the deviator stress and specific volume at critical state, respectively. M is a critical state parameter, and Γ is v_{CS} at $p' = 1$ MPa.

3)

The yield surface is the stress state when reached would result in plastic strain. Modified Cam clay has the yield surface defined as follows,

$$(5) \quad f = q^2 + M^2[p'(p' - p'_c)]$$

where, p_c' is the pre-consolidation pressure or maximum past pressure,

This MHBS model is capable of modeling the hydrate enhanced yielding strength and dilatancy. It also considers the impact of hydrate saturation, S_H, and how its effects are affected by straining via the introduction of the concept of mechanical hydrate saturation, SHmec, such that even with the same S_H the hydrates could have different effects. The important enhancements made for the MHBS model include,

1)

For an actual S_H, a mechanical hydrate saturation, SHmec, is introduced as (6)

$$(6) \quad SHmec = \chi \cdot SH$$

where χ is a degradation parameter, which is 1 for undeformed hydrate-bearing sediment, and becomes smaller as plastic shear strain accumulates. The degradation rate $d\chi$ is tied to the deviatoric plastic strain increment $d\varepsilon qp$ by a scale factor m as

$$(7) \quad d\chi = -m\chi d\varepsilon qp$$

2)

The presence of hydrates raises the volumetric yielding pressure, p'_{cd}, and enhances tensile strength, p'_{cc}, both expressed in a power form as follows,

$$(8) \quad p'_{cd} = a(SHmec)^b$$

$$(9) \quad p'_{cc} = c(SHmec)^d$$

3)

The introduction of subloading concept. Subloading is introduced to modify the Cam clay model to reflect the observation that plastic strain is induced even at low stress level. Together with the enhancement by hydrates, the subloading concept expands the modified Cam clay yield surface to become

$$(10) \quad f = q^2 + M^2(p' + pcc')[p' - R(pc' + pcd' + pcc')]$$

where $R \leq 1$ is a subloading coefficient that defines the distance separating the hydrate enhanced yield surface to the current stress state. R is further updated based on the plastic strain increment $|d\varepsilon p|$, with

$$(11) \quad dR = -u\ln(R)|d\varepsilon p|$$

where, u is a pre-yielding plasticity parameter.

Following the Cam clay construct, the elastic bulk modulus, K, can be found as K=νp'/κ. Additionally, either the shear modulus, G, or the Poisson ratio, μ, is a required input to complete the description of the elastic properties. Thus, the MHBS model adopted for the study has 12 parameters that include the Cam clay parameters of λ,κ, M, p'_c, the initial porosity φ_0, μ or G; the hydrate enhanced yielding pressure and strength parameters a, b, c, and $d;$ the hydrate degradation rate parameter, m; and the pre-yielding plasticity parameter of u from the subloading model.

4. Experimental data and model fit

Based on the geomechanical test data obtained from NGHP-02 core samples (Yoneda et al., this volume a), the 12 parameters of the model are determined. It is unprecedented that so many laboratory mechanical tests have been conducted on high quality pressure cores of marine sediment samples. The list of the available test data is summarized in Table 2, of which only the multistage triaxial tests were not used. The MHBS model parameters are calibrated to fit the test results and the parameters obtained are summarized in Table 3.

Table 2. Geomechanical tests performed (Yoneda, this volume a).

Type of test and designation	Sample number	Effective confining stress (MPa)	S_H
TACTT B Consolidation	16B-3P (273.81–273.89)	0.2–11	37.7 %
TACTT B Consolidation	16B-3P (274.14–274.23)	0.2–11	63.0 %
TACTT B Consolidation	16B-4P (277.22–277.30)	0.2–5	71.6 %
TACTT C Consolidation	16B-7P (287.12–287.20)	0.2–11	63.9 %
TACTT C Consolidation	16B-3P (274.03–274.13)	0.2–11	62.8 %
TACTT C Triaxial post dissociation	16B-7P (287.12–287.20)	12	0%
TACTT C Triaxial post dissociation	16B-3P (274.03–274.13)	12	0%
TACTT A Triaxial	16B-3P (274.46–274.56)	1	73.4 %
TACTT A Triaxial	16B-3P (273.61–273.69)	1	52.2 %
TACTT A Triaxial	16B-7P (286.48–	1.1	82.2

Type of test and designation	Sample number	Effective confining stress (MPa)	S_H
	286.56)		%
TACTT E Multistage Traixial	–	0.2, 0.5, 1, 3	63.5 %
TACTT E Multistage Triaxial	–	0.2, 0.5, 1, 3	0%

Table 3. Soil model parameters employed in analysis.

Parameters	Hydrate-Bearing Sands (Unit 4)	Mud (All Units)
Critical state Parameter M	1.20	1.31
Slope of compression line λ	0.087 (w/o GH): 0.078 (with GH)	0.20
Slope of swelling line, k	0.011	0.05
Poisson's ratio	0.35	0.23
Pre-yield plasticity u	1	960
Pre-consolidation pressure, p'_c	1.0 MPa	0.012 z (m) + 0.29 MPa
Initial porosity φo	0.4	0.3–0.7 (unit dependent)
Strength increase due to	2(SHME)1.1MPa	0

Parameters	Hydrate-Bearing Sands (Unit 4)	Mud (All Units)
hydrate, p'_{cc} (*a* and *b*)		
Dilation increase due to hydrate, p'_{cd} (*c* and *d*)	10(SHME)2.0MPa	0
Hydrate degradation factor *m*	1	0

The dominant mode of geomechanical response for this study is the compression of the sediment under depressurization. Consolidation data thus take priority in the calibration of the model parameters. The calibrated parameters are then used in modeling the two consolidation tests, denoted as TACTT-B and TACTT-C. In modeling the TACTT-B tests, we assume that the core sample had been unloaded from the in-situ p' of 1 MPa to the starting state of 0.2 MPa then reloaded to $p' = 1$ MPa, and after dissociation is induced there, the sample is further consolidated to 12 MPa. In modeling the TACTT-C consolidation test, we again consider that the sample had also been unloaded from the in-situ p' of 1 MPa to the starting state of 0.2 MPa then reloaded to $p' = 5$ MPa, and after dissociation is induced there, the sample is also consolidated to 12 MPa. The computed change in porosity versus the change in effective confining pressure are plotted together with test results in Fig. 3. The modeling results are deemed satisfactory in comparison with the test results.

(a) Dissociation at p'=1 MPa
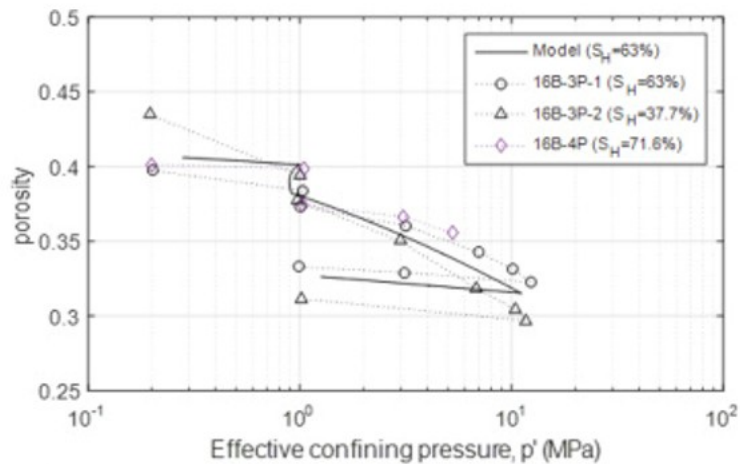
(b) Dissociation at p'=6 MPa
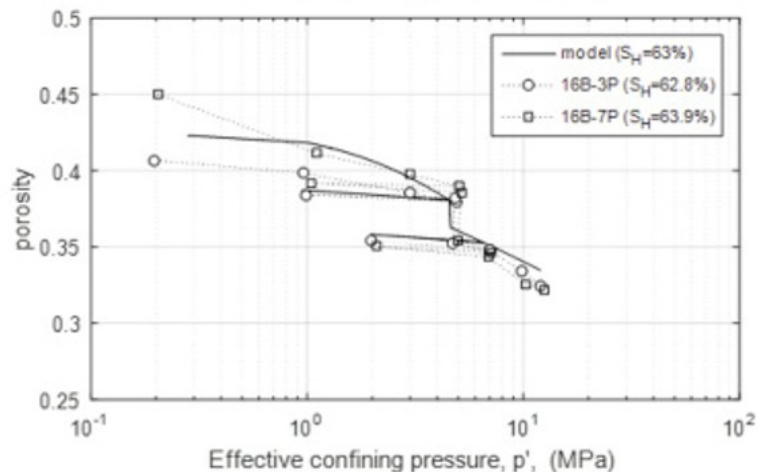
Fig. 3. Model versus the consolidation with dissociation test data: (a) dissociation at p' = 1 MPa; (b) dissociation at p' = 5 MPa.

There are three sets of triaxial compression tests among them two are conventional triaxial tests, and one is multistage tests. The TACTT-A tests are

conventional triaxial tests which included three hydrate-bearing soil samples with hydrate saturation, S_H, of 55.2%, 73.4% and 82.2%, respectively. The test results, except for the set with $S_H = 73.4\%$, show that the samples exhibited small or negligible dilation, and thus no strain softening is observed after failure. However, the $S_H = 73.4\%$ sample, which has strength comparable to that of $S_H = 82.2\%$, exhibits strong dilatancy. Because of the contradiction in the data, during the calibration, trade-offs have to be made. Two considerations enter the decision: First, the areas close to the wellbore are locations where potential instability might be of concern and good estimates of strength are required. Second, under the depressurization, the resulted dissociation would substantially reduce hydrate saturation of the sediment from in-situ values in the near field. Put these two together, the study thus focuses on fitting the results from the lowest hydrate saturation of $S_H = 55.5\%$, and as both the $S_H = 55.5\%$ and 82.2% samples exhibit negligible dilatancy, a decision is also made to disregard the dilatancy of the $S_H = 73.4\%$ data. As a result, the model fits the $S_H = 55.5\%$ stress-strain data, but only the strength of the $S_H = 73.4\%$ data. The strength of $S_H = 82.2\%$ projected by the model, based on these considerations, is higher than the test result. Yun et al. (2007) has shown that strength of tetrahydrofuran hydrate bearing soils would steadily increase even up to $S_H = 100\%$. But most other laboratory tests on MHBS only prepared samples up to about $S_H = 60\%$ (e.g., Miyazaki et al., 2011), and it is not clear if the present data imply that the strength of MHBS increases with S_H would hit a plateau when S_H reaches as high as 70–80%. For the study, this is not a critical issue for the reasons given above. Fig. 4 presents the comparisons of the test and modeled results of these three samples. How does the decision affect the estimation of results when hydrates are completely dissociated? TACCT-C are the second set of triaxial compression tests which were conducted on completely dissociated and thus hydrate-free samples at the end of consolidation-dissociation-consolidation tests, and the samples were sheared to failure under $p' = 12$ MPa. Two sets of results are available: one is dissociated at $p' = 1$ MPa, the other at $p' = 6$ MPa, and they show different dilatancy characteristics but similar strengths. The value of p' at which dissociation took place does not appear to significantly affect the shear stress-shear strain curves. The modeling results show the model gives larger modulus but only about 10% larger in strength (Fig. 5).
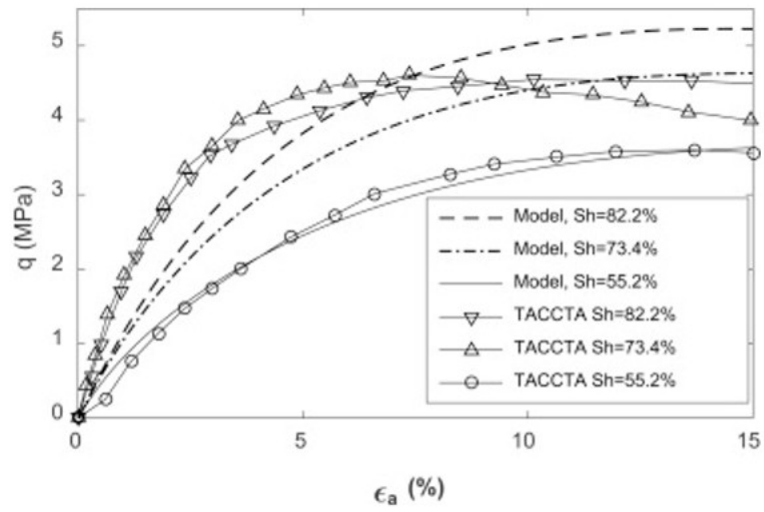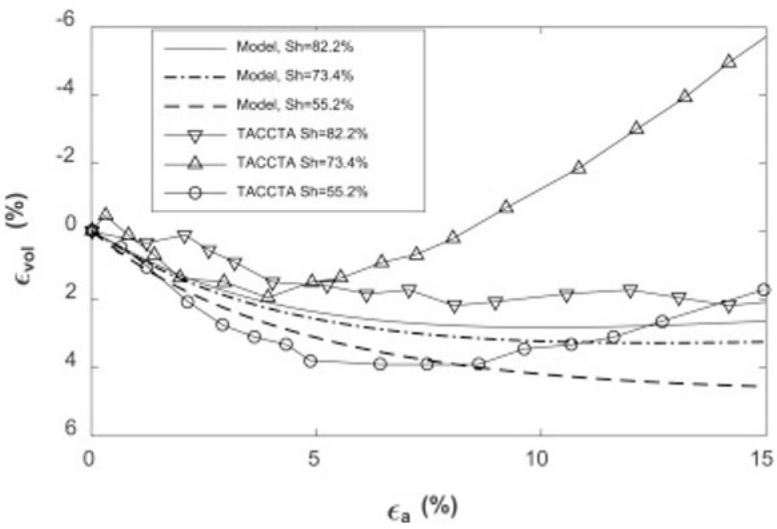
Fig. 4. Model versus drained triaxialtest results with p' = 1 MPa (a) q versus ε_a (b) ε_{vol}versus ε_a.
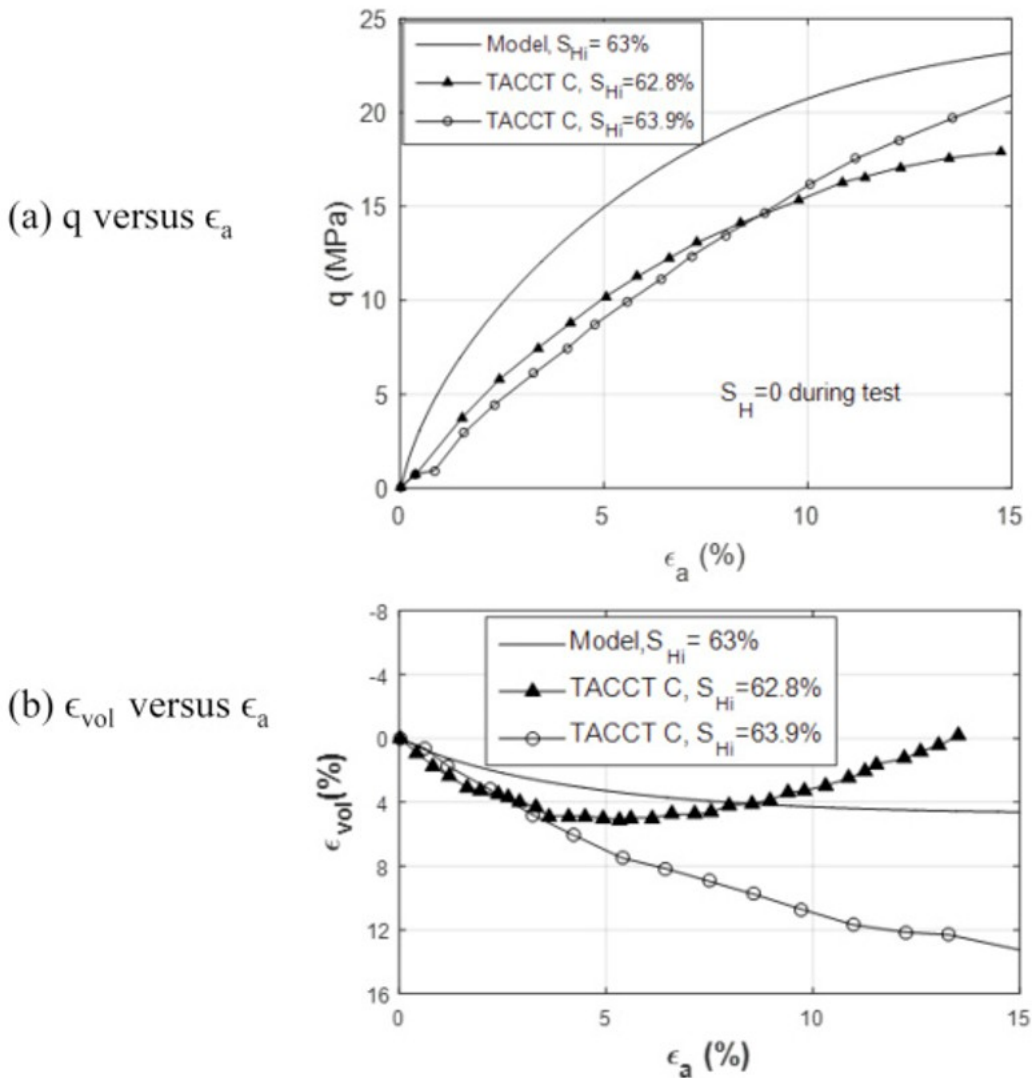
Fig. 5. Model versus drained triaxial test results conducted after hydrate dissociation with p' = 12 MPa (a) q versus ε_a, (b) ε_{vol} versus ε_a.

The third set of triaxial compression tests, TACCT-E, consists of two multi-stage triaxial tests on two different samples, one has $S_H = 63.5\%$ and the other is hydrate-free. The set with $S_H = 63.5\%$ gives erratic results for p' up to 1 MPa, and thus calls into question the data reliability. The sample without hydrate, as a result of dissociated from $S_H = 71.6\%$, shows a steady trend of strength increase with confining pressure, and it gives higher strength than those obtained from the conventional triaxial tests, TACTT-A. In this study, the conventional triaxial test data are given more weight and thus model predicts lower strength in comparison with the multistage test data as depicted in Fig. 6. As a reference, Fig. 7 shows that data from the literature, using Toyoura sands and Nankai Trough core samples, gives higher strength than those obtained for Site 16. The noticeable difference between the literature specimens and those collected at NGHP-02 Site 16 is the relatively

high fines content at NGHP-02 Site 16, for which some samples have fines concentrations as high as 35%. With higher fine contents of the sediments, the relative lower strength is expected.
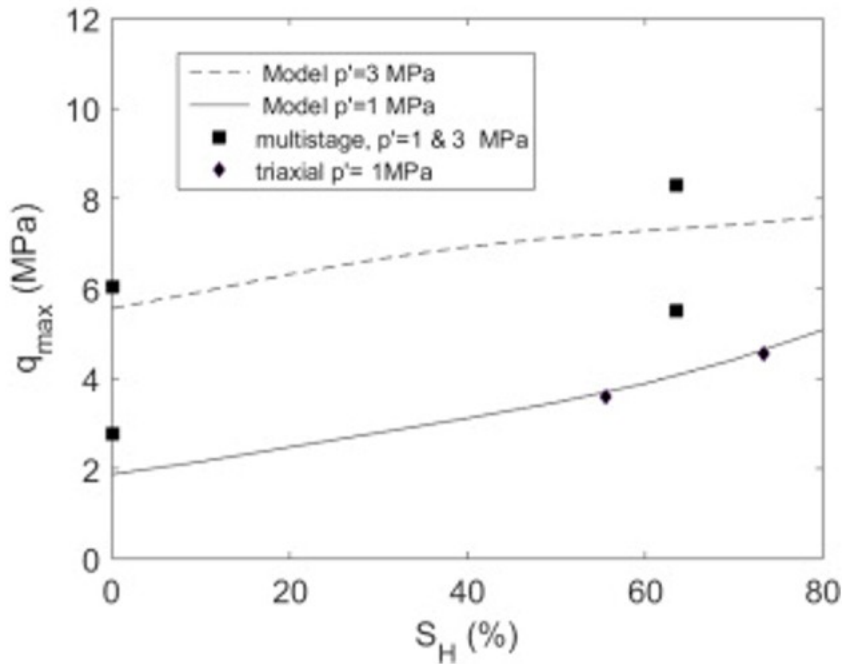

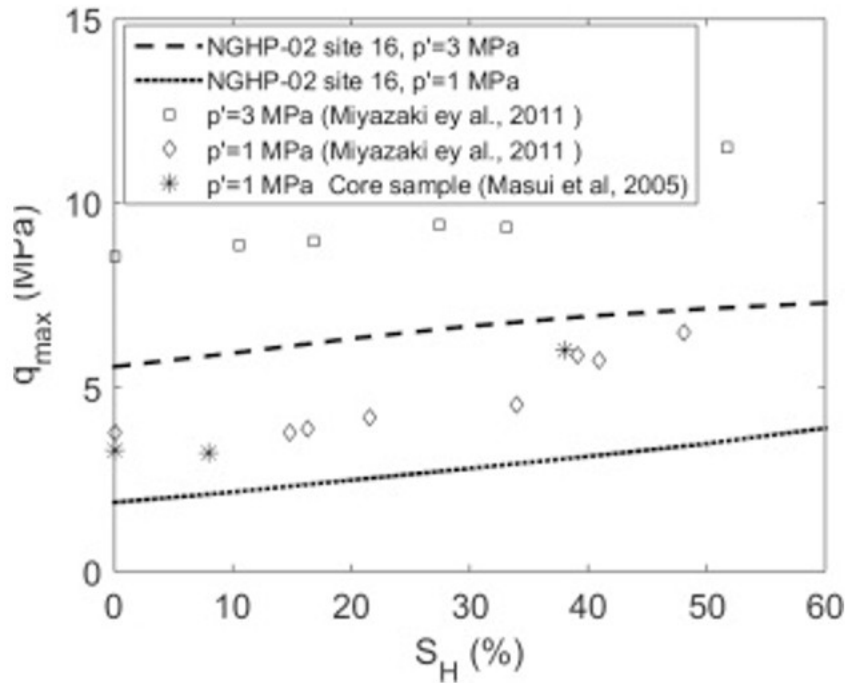Fig. 6. Model predicted strength versus available data.

Fig. 7. Model predicted strength versus several sets of data.

No data are available for the overburden mud and for the fine-grained Site 16 interbedded mud layers. For mud modeling, we use the laboratory tests

by Nishio et al. (2009) that consists of three undrained triaxial tests on samples recovered from different depths below seafloor at the Nankai Trough site. The model fit provides a general trend of the stress-strain curve and pore pressure development pattern, but does not give a detailed fit. However, the overburden responses are not sensitive to the precise stress-strain behavior in the muds. As the analysis presented later demonstrates, the sediments above the hydrate reservoir generally is subjected to very small strain, and mostly remained elastic.

To complete the model parameter discussion, it is important to mention that the most important impact of porosity reduction in the sediment due to depressurization is that it results in permeability reduction and that, in turn, affects the gas production. For the flow study, the permeability change caused by porosity change is modeled by (Davies and Davies, 1999; Rutqvist et al., 2002),

$$(12) \quad k = k_0 \exp[\gamma(\varphi/\varphi_0 - 1)]$$

where, k_0 and φ_0 are initial intrinsic permeability and porosity, respectively, and γ is the parameter controlling the sensitivity of permeability on sediment compaction. Two values of γ have been used in the flow study, they are $\gamma = 4.6$ and $\gamma = 17.2$. A detailed discussion on the determination of γ can be found in Myshakin et al. (this volume).

5. Problem setup and cases studied

The problem is modeled as axi-symmetric within the region of study (Fig. 8) which extends 300 m radially from the wellbore, and 400 m vertically from the seafloor. The geomechanical modeling uses a relatively coarse vertical mesh with 44 layers in Unit 4, in which the thinnest layer is 0.2 m thick, whereas the flow study employs 241 layers for Unit 4 each of 0.1 m in thickness. Overall, this study uses a total of 192 layers in the vertical direction and 167 subdivisions in the radial directions, with 28 of the divisions lie within 20 m distance from the wellbore. On the other hand, the corresponding flow study analyzes a larger domain of 500 m by 500 m that consists of 355 layers and 101 subdivisions, and has 58 divisions lie within 20 m from the wellbore. The pore pressure and hydrate saturation results from the flow study are mapped to the geomechanical domain through interpolation.
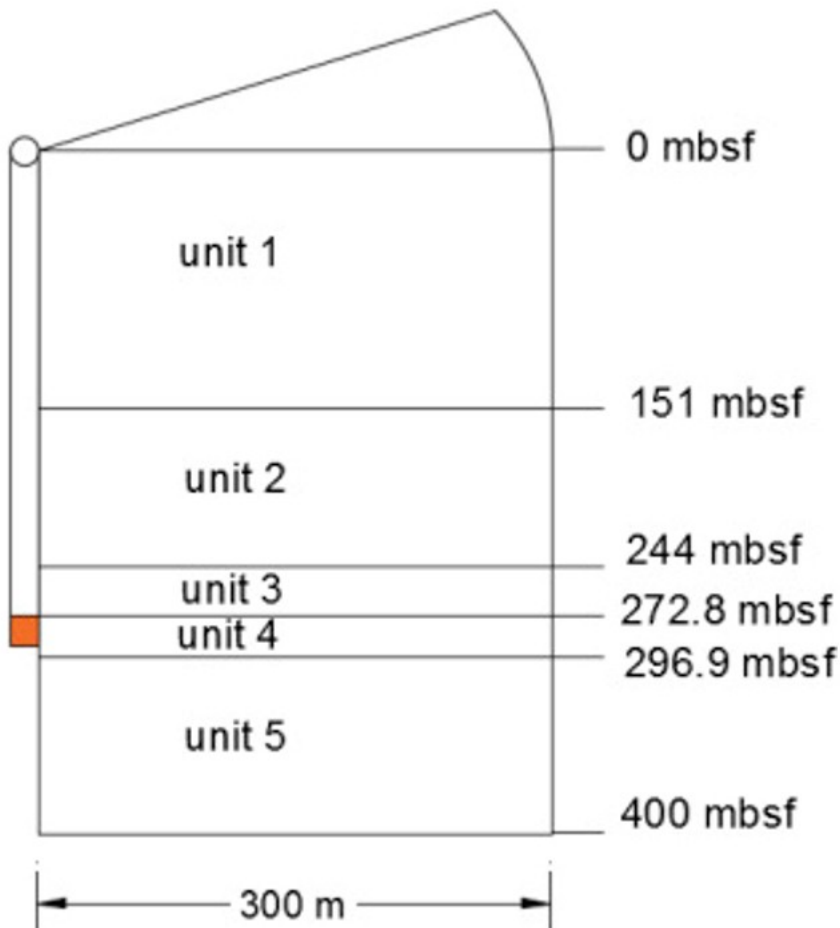
Fig. 8. The axi-symmetric domain for geomechanical study with the depressurization well on the left and its open section marked.

The borehole wall is modeled as a rigid wall which does not move or deform horizontally by assuming that there is perfectly effective sand control at the open-hole completion and no material is allowed to pass into the borehole. Essentially, the wellbore and the far field lateral boundaries are modeled as roller boundary, that is, they are constrained from moving laterally but free to move vertically. The bottom boundary was constrained from moving vertically. The top boundary of the model is the seafloor, where the pressure from the 2546.5 m of overlying seawater was applied in addition to the atmospheric pressure. The sediment in-situ is considered to be in static equilibrium. The unit weight of each unit is listed in Table 1. The initial pore water pressure is treated as hydrostatic based on the sea surfacelevel. The critical state parameter M of 1.2, corresponds to a friction angle of 30°. For the normal consolidated hydrate reservoir of Unit 4 this gives the coefficient of the at-rest earth pressure, K_0, of 0.5. The study further adopts this value for all the units. The geomechanical model used is designed to capture a simplified yet reasonable input model based on logging data collected during NGHP-02. The initial effective intrinsic permeability is set to 10 md for the reservoir hydrate-bearing sands, which is consistent with laboratory analyses

of NGHP-02 Site 16 cores (see Boswell et al., this volume; Myshakin et al., this volume). The case in which the permeability reduction parameter, γ, is set to 4.6 is presented herein, which represents a more critical case from geomechanical consideration as the depressurizationzone extends farther laterally than that by using γ = 17.2. After 90 days of production, the pressure and the hydrate saturation within the reservoir obtained for the case (Myshakin et al., 2018) are summarized in Fig. 9 where the impact is mostly confined to within 100 m laterally from the well. The 90-day results are presented because the flow study results show that gas production rate increases within the first 60 days then it hits a plateau. Also the interest herein is on the response during the early stage since this exploration is not expected to be carried out for a long time.
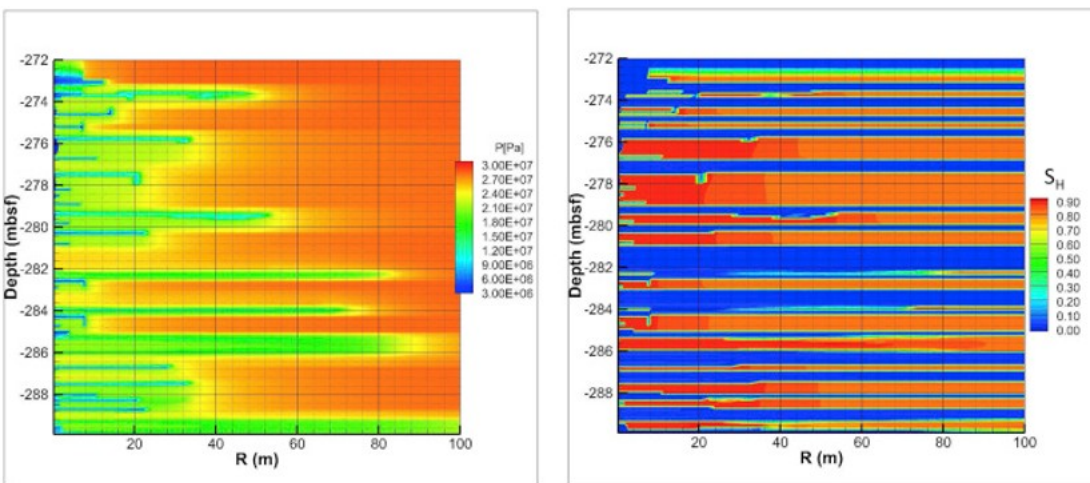
(a) The pressure distribution   (b) The hydrate saturation distribution

Fig. 9. The pressure and hydrate saturation distribution within the reservoir after 90 days of depressurization.

6. Results and discussion

The depressurization through the open section of the well leads to a depressurization that is confined within the reservoir from the first to the seventeenth hydrate-bearing sand layer within Unit 4, i.e., from 272.8 to 289.8 mbsf. Depressurization depends on brine withdrawal from the reservoir. There is only limited pressure drop beyond the reservoir due to low permeability of bounding mud layers.

For the study, the detailed movement patterns obtained are summarized in two figures. Fig. 10 gives the contours of the vertical movements of the sediment and five profiles of how they vary with distance at 2, 5, 10, 30, and 120 m laterally away from the wellbore. Fig. 11provides similar information for the lateral movement. Fig. 12 further gives a detailed view showing the displacement vector within Unit 4 and the resulting volumetric
strain showing a pattern affected by the pressure distribution. From Fig. 11, the settlement of the sediment are found to be maximum close to the

wellbore and become smaller away from it. The compression of Unit 4 drags down Unit 3, which results in the greatest downward movement at its bottom and reducing vertical movement upward. The maximum settlement on the seafloor is about 1.7 cm, whereas the vertical compaction just above the production unit obtained is about 73.5 cm, and the maximum heave of about 58.9 cm at the bottom of the production unit. There exists a transition zone within Unit 4 where there is negligible vertical movement. Near the wellbore, the lateral movement is constrained by the rigid well boundary. Fig. 11 shows that between 10 and 30 m away from the well, the lateral movement is largest and it reaches its peak value of 14.5 cm at 16 m from the well. Within that 10–30 m range, the movement concentrates mainly within the depressurized zone. Further away from the well, the lateral movement reduces but at the same time also spreads beyond the depressurized zone.
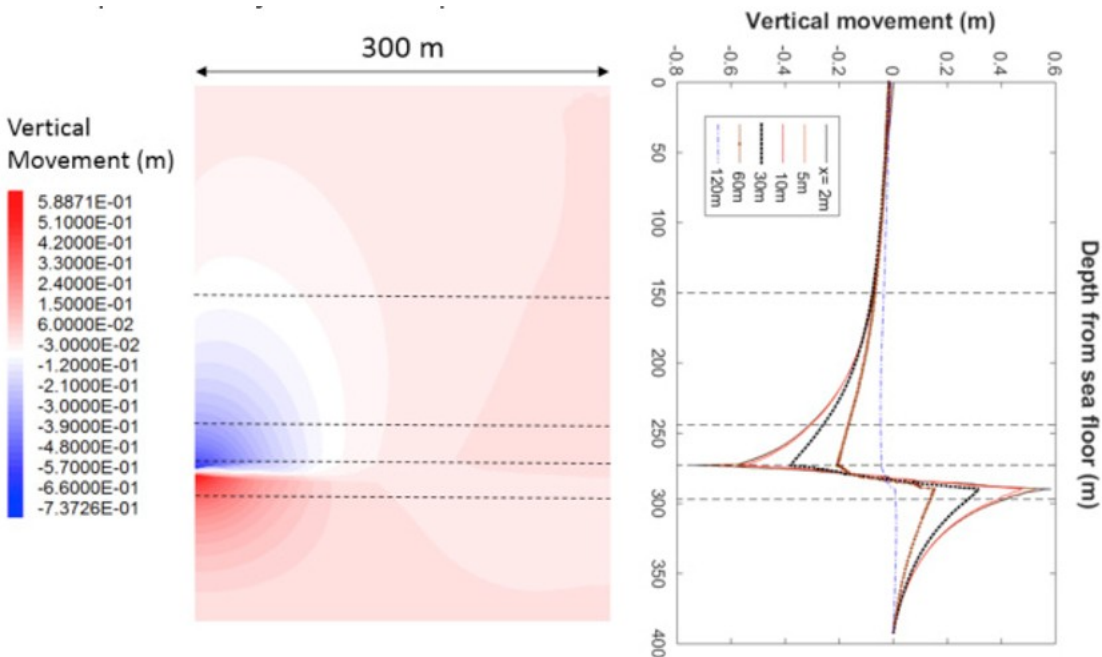
Fig. 10. The vertical movement of the sediment and its contours 90 days after gas production (settlement is negative).
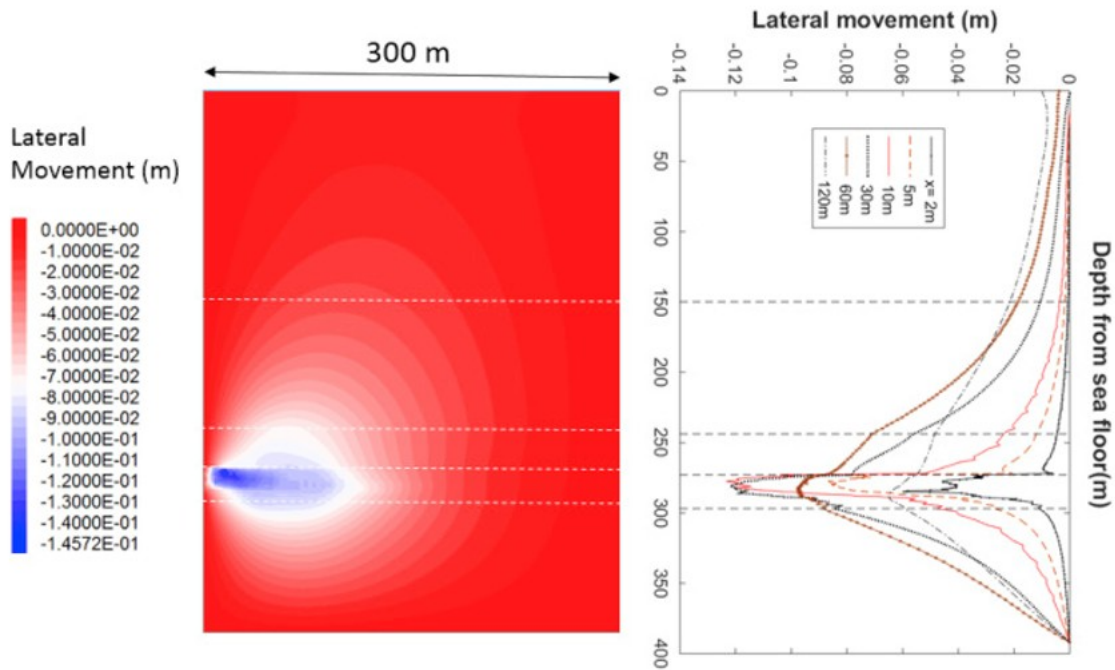
Fig. 11. The lateral movement of the sediment and its contour 90 days after production starts (moving toward well is negative).
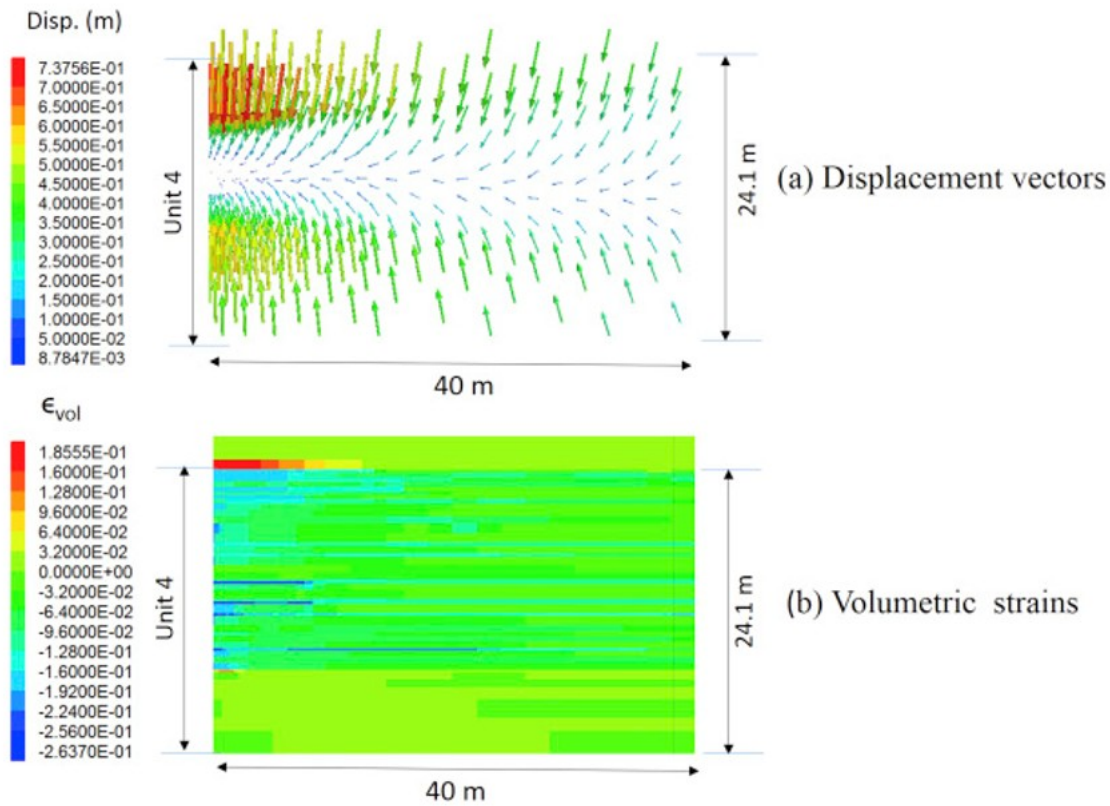

Fig. 12. (a) Displacement and (b) volumetric strain 90 days after depressurization started. Tension strain is positive.

The general pattern of the sediment movement due to depressurization of part of a thin reservoir stratum representative of the study is illustrated with a schematic plot in Fig. 13. It can readily be appreciated that the compression of the stratum will pull in the surrounding sediments toward the depressurized zone which are at their maximum close to the wellbore. This explains that in the near field, both the settlement and heave above and below depressurization zone of Unit 4 are at their peaks, and they diminish with distance from the wellbore. This creates a stretching that results in both the units above and the unit below Unit 4 to subject to tensile volumetric strain. On the perimeter of the depressurization zone, areas near the edge of the largest pressure drop experience the largest tensile strains. Fig. 12(b) shows that they take place on the interface between Unit 3 and Unit 4, and, to a lesser extent, below the seventeenth hydrate-bearing sand layer.
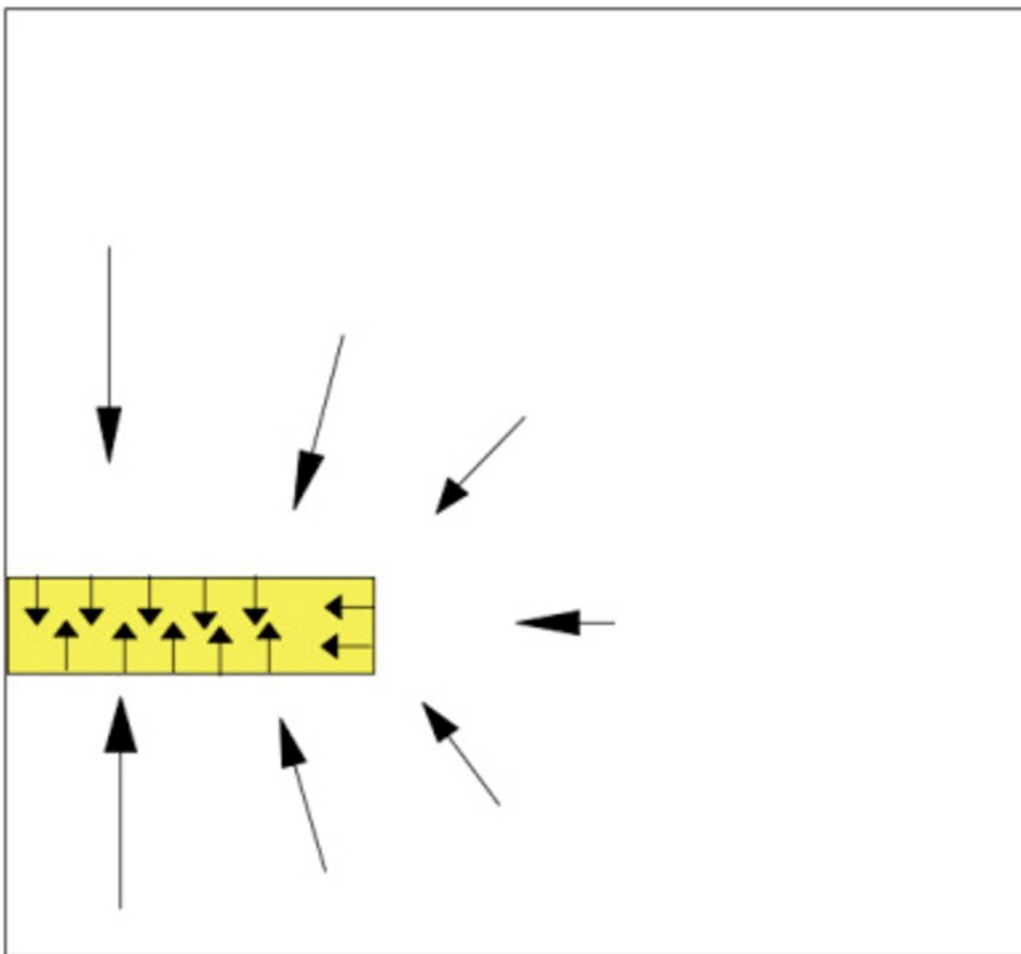

Fig. 13. A schematic plot of the sediment deformation pattern due to depressurization of a hydratereservoir.

In the depressurized zone, the sediment stability, from the perspective of shear strength, experiences two opposing effects during depressurization. On the one hand, because depressurization raises the effective confining pressure, the soil strength is raised and should become more stable. On the

other, depressurization causes hydrate dissociation and thus reduces the in-situ strength from that of hydrate-bearing to that of hydrate-free sand. When the confining pressure is high, the strength differentials between MHBS and hydrate-free sediments become small (Yoneda et al., 2017). Thus, the net effect of depressurization would not introduce instability from strength consideration. But there are some areas immediately above and below the depressurization zone, where large tensile strains have been observed, indicating the loss of effective confining pressure due to tension. To investigate if this should be a concern, the regions where such p' reduction leads to critical value with q/p'>M are found and plotted in Fig. 14. Altogether there are three such areas as shown in light color. Furthermore, stress paths at two such q/p'>M locations, are plotted as Points A and C, respectively, with one above and the other below the depressurized zone. For comparison, Point B is taken from the highly pressurized hydrate-bearing sand layer. A stress path is a plot that shows how stress state evolves under loading. The stress paths connect the initial stress state, and the stress states at 10, 30, 60 and 90 days after production are presented in Fig. 15. The locations of the three points are also marked on Fig. 14, where Point A is located at r = 15.2 m, z = 272.4 mbsf, Point B at r = 1.14m, z = 284.1 mbsf, and Point C at r = 2.98 m, z = 289.9 mbsf. Initially, the stress states of all three points do not differ much. Once production starts, it clearly shows that Points A and C move toward the left because they are subjected to tension, where Point B moves to the right because of compression. Both Points A and C have been strained passed their peak strength and become softened and with further loading they may enter critical state. Since they are contained by neighbors, no excessive shear strain development is expected upon further straining. As such, these isolated spots have insignificant impact on overall stability of the sediment. Whereas, Point B being highly depressurized remains stable, as its stress path shows a steady increase in effective confining pressure that is accompanied by a lesser deviatoric stress increase.
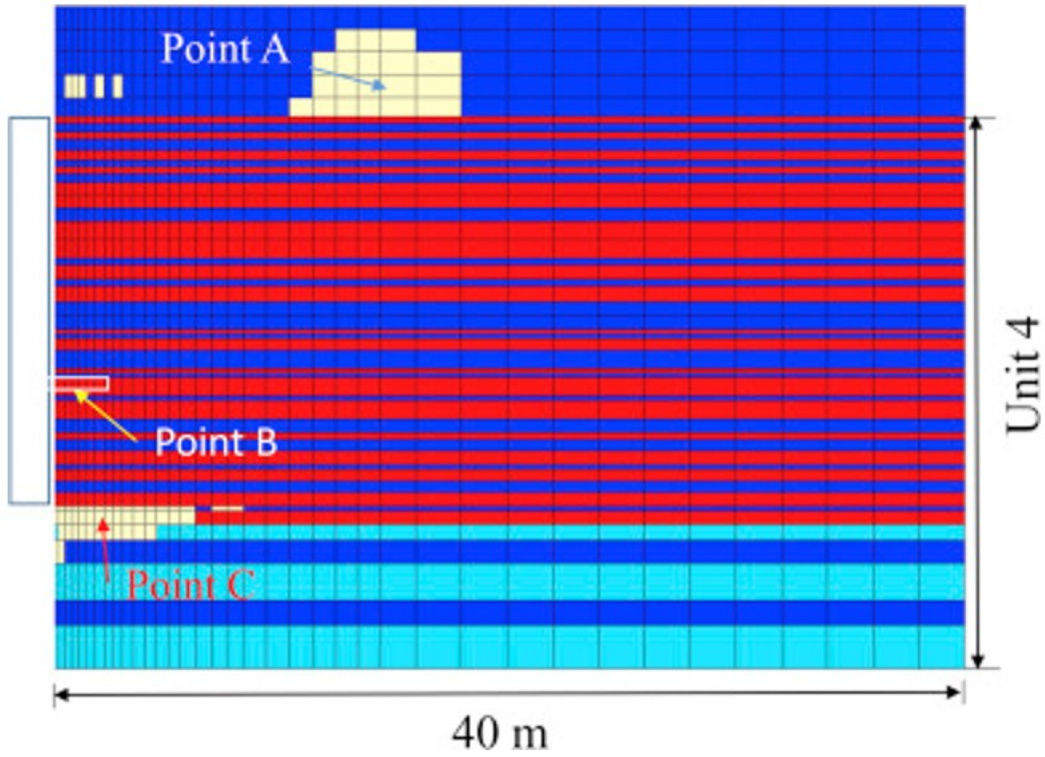
Fig. 14. Zones of different q'/p ratio. Shown in whites are three isolated area in the whole domain of study where q/p'>M, and two of them are marked as Points A and C, while Point B represents a highly pressurized zone. (On the left is depicted the open section of the well which corresponds to the depressurization zone).
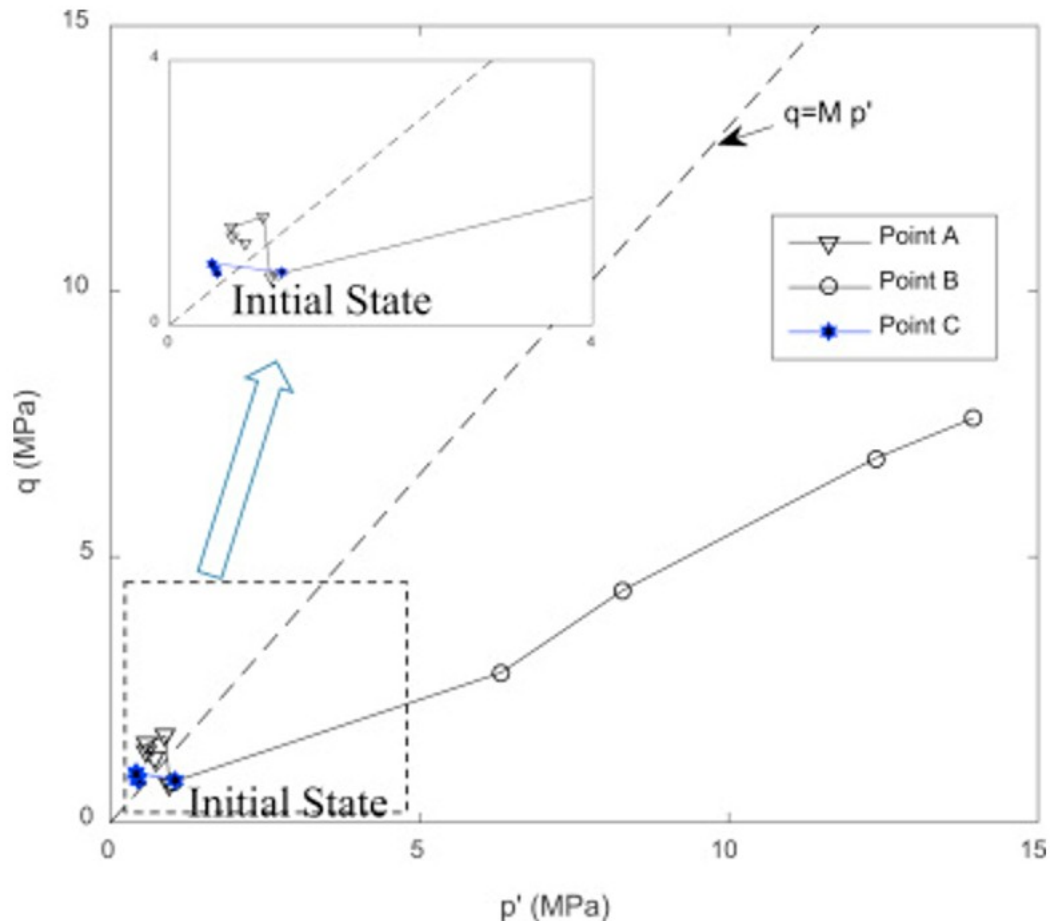
Fig. 15. Stress paths at three locations marked in Fig. 14.

To assess the accuracy of the one-way coupling approach adopted here, the question to be answered is: does the flow study project a porosity change during depressurization compatible with those obtained from geomechanical analysis? To answer this question, the pore compressibility α that links the flow and geomechanical studies is back-computed from the geomechanical study results. Using all of the hydrate-bearing sand layer deformation data that have pressure drops greater than 20 MPa, α is back-computed for each element from the volume strain and pressure change and plotted in Fig. 16. While the flow study uses $\alpha=1.3\times10-8(Pa^{-1})$, the mean back-computed α is $1.39\times10-8(Pa^{-1})$. These two values can be considered to be in good agreement. Using $\alpha=1.3\times10-8(Pa^{-1})$, and with an initial porosity, $\varphi0 = 0.4$, under a pressure increase of 20 MPa, the reduced porosity, φ, would be 0.3084. The permeability reduction would be $k/k0 = 0.349$ given this porosity change with $\gamma=4.6$. On the other hand, when $\alpha=1.39\times10-8(Pa^{-1})$ was used, under the same conditions, φ would be 0.3029, yielding $k/k0 = 0.327$. This shows that the two different values of α represent a less than 5% difference in the calculated permeability. Thus this provides a justification of using $\alpha=1.3\times10-8$ (Pa^{-1}) for pore

compressibility in the flow study, and supports the one way coupling approach adopted for the study.
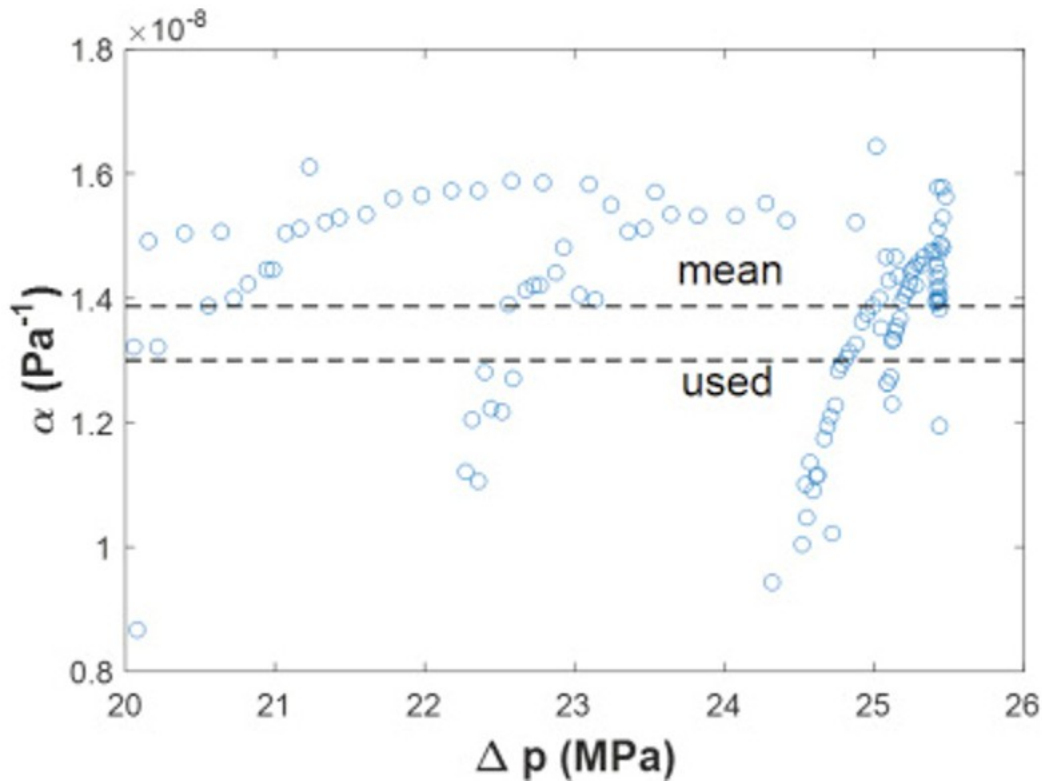

Fig. 16. Pore compressibility, α, back computed from the geomechanicalanalysis results.

7. Conclusions and summary

This study presents a geomechanical analysis of a marine sediment response to methanegas production via depressurization at NGHP-02 Site 16 offshore eastern India. The site has two standout features: one is that the hydrate reservoir is deeply located at 2819.3 m to 2843.4 m below the sea level, and the other is that the reservoir is composed of thin layers of hydrate rich sand strata interbedded with mud layers. These conditions present different challenges to modeling. Because of the depth, using depressurization as means for gas production would require an unprecedented level of pore pressure drop which can be as high as 25 MPa. Whereas the interbedded thin layers of hydrate rich sands and muds of the reservoir means very fine mesh is needed in order to accurately estimate gas production, that is, however, not compatible with viable geomechanical modeling. Thus, the study has taken the route of a one-way coupled flow-geomechanical analysis scheme. The essence of coupling is, however, captured by making use of pore compressibility for the flow study to reflect the porosity change that the geomechanical response of the deposit would generate. This pore compressibility used is, at the end, cross-checked and validated with results from the geomechanical study.

The study makes use of the availability of laboratory geomechanical test data on high quality pressure core samples. This facilitates calibration of the subloading critical state MHBS constitutive model used for the study and provides support to the modeling assumptions and results. This is the first time that such high quality hydrate-bearing sediment test data from a marine environment are available for incorporating into analysis. However, it is also noted that the tests were conducted well below the 25 MPa effective confining stress levels targeted in this study for NGHP-02 Site 16. This study thus assumes parameter dependencies on effective stress can be extrapolated to effective stresses nearly double what was used in the measurements themselves. The depressurization requirements of NGHP-02 Site 16 demonstrate a need for mechanical property measurements at effective confining stresses reaching 25 MPa. Devices to accomplish such testing on hydrate-bearing material are being developed, and some of the initial results are presented in Yoneda et al. (this volume b).

This study concludes that, assuming elimination of sand production through well designed sand control completion, the sediment remains stable within the gas production period studied.

Acknowledgements

References

Boswell et al., this volume

Boswell, R., Collett, T., Moridis, G., Myshakin, E., Ajayi, T., Seol, Y. this volume, Geologic models for gas hydrate reservoir simulations of finely-interbedded sand-mud sequences: an example from Site NGHP-02-16, offshore India. Mar. Petrol. Geol.

Collett et al., this volume

Collett, T., Kumar, P., Singh, S., Chopra, K., et al., this volume, India national gas hydrate Program expedition 02 – scientific results. Mar. Petrol. Geol.

Davies and Davies, 1999

J.P. Davies, D.K. Davies**Stress-dependent permeability: characterization and modeling**

SPE Annual Technical Conference and Exhibition, 3-6 October, Houston, Texas (1999)

Hyodo et al., 2014

M. Hyodo, Y. Li, J. Yoneda, Y. Nakata, N. Yoshimoto, A. Nishimura**Effects of dissociation on the shear strength and deformation behavior of methane hydrate-bearing sediments**

Mar. Petrol. Geol., 51 (2014), pp. 52-62

Itasca Consulting Group, 2012

I. Itasca Consulting Group**FLAC3D — Fast Lagrangian Analysis of Continua in Three-dimensions, Ver. 5.0, Minneapolis: Itasca**

(2012)

Jeong-Hoon et al., 2014

J-H Choi, D. Sheng, J-H Cha, S. Yongkoo**Laboratory formation of noncementing hydrates in sandy sediments**

G-cubed, 15 (2014), pp. 1648-1656

Kim et al., 2012

J. Kim, G.J. Moridis, J. Rutqvist**Coupled flow and geomechanical analysis for gas production in the Prudhoe Bay Unit L-106 well Unit C gas hydrate deposit in Alaska**

J. Petrol. Sci. Eng., 92–93 (2012), pp. 143-157

Klar et al., 2013

A. Klar, S. Uchida, K. Soga, K. Yamamoto

Explicitly Coupled Thermal Flow Mechanical Formulation for Gas-hydrate Sediments, vol. 18 (2013), pp. 196-206

CrossRefView Record in Scopus

Kumar et al., this volume

Kumar, P., Collett, T., et al., this volume, India national gas hydrate Program expedition 02 – operational and technical summary. Mar. Petrol. Geol.

Lin et al., 2015

J.-S. Lin, Y. Seol, J-H. Choi**An SMP critical state model for methane hydrate-bearing sands**

Int. J. Numer. Anal. Meth. GeoMech., 39 (2015), pp. 969-987

Masui et al., 2005

A. Masui, H. Haneda, Y. Ogata, K. Aoki**Effects of Methane Hydrate Formation on Shear Strength of Synthetic Methane Hydrate Sediments, the Fifteenth International Offshore and Polar Engineering Conference**

International Society of Offshore and Polar Engineers, Seoul, Korea (2005)

Miyazaki et al., 2011

K. Miyazaki, A. Masui, Y. Sakamoto, K. Aoki, N. Tenma, T. Yamaguchi**Triaxial compressive properties of artificial methane-hydrate-bearing sediment**

J. Geophys. Res., 116 (2011), p. B06102

Moridis et al., 2011

G. Moridis, T.S. Collett, M. Pooladi-Darvish, S.H. Hancock, C. Santamarina, R. Boswell, T.J.Kneafsey, J. Rutqvist, M.B. Kowalsky, M.T. Reagan, E.D. Sloan, A. Sum, C. Koh**Challenges, Uncertainties, and Issues Facing Gas Production from Gas-hydrate Deposits**

(2011)

Moridis et al., 2008

G. Moridis, M. Kowalsky, K. Pruess**TOUGH+Hydrate v1.0 User's Manual: a Code for the Simulation of System Behavior in Hydrate-bearing Geologic Media**

Lawrence Berkley National Laboratory, Berkley, California (2008)

Myshakin et al., this volume

Myshakin, E., Lin, J.-S., Uchida, S., Seol, Y., Collett, T., Boswell, R., this volume, Numerical simulation of depressurization-induced gas production from an interbedded turbidite hydrate-bearing sedimentary section in the offshore of India: site NGHP-02-16 (Area-B). Mar. Petrol. Geol.

Nishio et al., 2009

S. Nishio, E. Ogisako, A. Denda**Geotechnical properties of core samples recovered from seabed ground in east Nankai Trough**

J. Geogr., 118 (2009), pp. 955-968

Roscoe and Burland, 1968

K.H. Roscoe, J.B. Burland**On the generalized stress strain behaviour of wet clay**

J. Heyman, F.A. Leckie (Eds.), Engineering Plasticity, Cambridge University Press, Cambridge, England(1968), pp. 535-609

Rutqvist, 2017

J. Rutqvist**An overview of TOUGH-based geomechanics models**

Comput. Geosci., 108 (2017), pp. 56-63

Rutqvist et al., 2009

J. Rutqvist, G. Moridis, T. Grover, T. Collett**Geomechanical response of permafrost-associated hydrate deposits to depressurization-induced gas production**

J. Petrol. Sci. Eng., 67 (2009), pp. 1-12

Rutqvist and Moridis, 2009

J. Rutqvist, G.J. Moridis**Numerical studies on the geomechanical stability of hydrate-bearing sediments**

SPE J., 14 (2) (2009)

Rutqvist et al., 2012

J. Rutqvist, G.J. Moridis, T. Grover, S. Silpngarmlert, T.S. Collett, S.A. Holdich**Coupled multiphase fluid flow and wellbore stability analysis associated with gas production from oceanic hydrate-bearing sediments**

J. Petrol. Sci. Eng., 92–93 (2012), pp. 65-81

Rutqvist et al., 2002

J. Rutqvist, Y.S. Wu, C.F. Tsang, G. Bodvarsson**A modeling approach for analysis of coupled multiphase fluid flow, heat transfer, and deformation in fractured porous rock**

Int. J. Rock Mech. Min. Sci., 39 (2002), pp. 429-442

Schofield and Wroth, 1968

A.N. Schofield, C.P. Wroth**Critical State Soil Mechanics**

McGraw-Hill, London (1968)

Shukla et al., this volume

Shukla, K., Kumar, P., Collett, T., Boswell, R., Frye, M., Riedel, M., Pandey, B., Kaur, I., Vishwanath, K., this volume, National Gas Hydrate Program Expedition 02 in the offshore of India: pre-expedition drill site evaluation in the Krishna-Godovari deep offshore. Mar. Petrol. Geol.

Uchida et al., this volume

Uchida, S., Lin, J.-S., Myshakin, E.M., Seol, Y., Boswell, R., this volume, Numerical simulation of sand migration in interbedded hydrate-bearing sediments at Site NGHP-02-16. Mar. Petrol. Geol.

Uchida et al., 2012

S. Uchida, K. Soga, K. Yamamoto**Critical state soil constitutive model for methane hydrate soil**

J. Geophys. Res., 117 (2012), p. B03209

Waite et al., 2009

W.F. Waite, J.C. Santamarina, D.D. Cortes, B. Dugan, D.N. Espinoza, J. Germaine, J. Jang, J.W. Jung, T.J. Kneafsey, H. Shin, K. Soga, W.J. Winters, T.S. Yun**Physical properties of hydrate-bearing sediments**

Rev. Geophys., 47 (2009), p. RG4003

Yamamoto et al., 2014

K. Yamamoto, Y. Terao, T. Fujii, T. Ikawa, M. Seki**Operational overview of the first offshore production test of methane hydrates in the Eastern Nankai Trough. OTC-25243-MS**

Offshore Technology Conference, Houston, TX, 5-8 May (2014)

Yoneda et al., 2017

J. Yoneda, A. Masui, Y. Konno, Y. Jin, M. Kida, J. Katagiri, J. Nagao, N. Tenma**Pressure-core-based reservoir characterization for geomechanics: insights from gas hydrate drilling during 2012–2013 at the eastern Nankai Trough**

Mar. Petrol. Geol., 86 (2017), pp. 1-16

Yoneda et al., this volume a

Yoneda, Y., Oshima, M., Kida, M., Kato, A., Konno, Y., Jin, Y., Tenma, N., Waite, W., Jang, J., this volume a, Pressure core based analysis of mechanical properties of hydrate-bearig sedimentsrecovered during India's India National Gas Hydrate Program Expedition, NGHP-02. Mar. Petrol. Geol.

Yoneda et al., this volume b

Yoneda, J., Masui, A., Konno, Y., Jin, Y., Kida, M., Katagiri, J., Nagao, J., Tenma, N., this volume b, Consolidation and hardening behavior of hydrate-bearing pressure core sediments under high confining pressure based on natural core sample from NGHP-02. Mar. Petrol. Geol.

Yun et al., 2007

T.S. Yun, J.C. Santamarina, C. Ruppel**Mechanical properties of sand, silt, and clay containing tetrahydrofuran hydrate**

J. Geophys. Res., 112 (2007), p. B04106